



**HAL**  
open science

## An improved analysis of the N<sub>2</sub>O absorption spectrum in the 1.18 $\mu\text{m}$ window

E.V. Karlovets, S.A. Tashkun, S. Kassi, A. Campargue

► **To cite this version:**

E.V. Karlovets, S.A. Tashkun, S. Kassi, A. Campargue. An improved analysis of the N<sub>2</sub>O absorption spectrum in the 1.18  $\mu\text{m}$  window. *Journal of Quantitative Spectroscopy and Radiative Transfer*, 2022, 278, pp.108003. 10.1016/j.jqsrt.2021.108003 . hal-03865541

**HAL Id: hal-03865541**

**<https://hal.science/hal-03865541>**

Submitted on 22 Nov 2022

**HAL** is a multi-disciplinary open access archive for the deposit and dissemination of scientific research documents, whether they are published or not. The documents may come from teaching and research institutions in France or abroad, or from public or private research centers.

L'archive ouverte pluridisciplinaire **HAL**, est destinée au dépôt et à la diffusion de documents scientifiques de niveau recherche, publiés ou non, émanant des établissements d'enseignement et de recherche français ou étrangers, des laboratoires publics ou privés.

# An improved analysis of the N<sub>2</sub>O absorption spectrum in the 1.18 μm window

E.V. Karlovets<sup>1\*</sup>, S.A. Tashkun<sup>2</sup>, S. Kassi<sup>3</sup>, A. Campargue<sup>3\*</sup>

<sup>1</sup> Tomsk State University, Laboratory of Quantum Mechanics of Molecules and Radiative Processes, 36, Lenin Avenue, 634050, Tomsk, Russia

<sup>2</sup> V.E. Zuev Institute of Atmospheric Optics, 1, Academician Zuev square, 634055 Tomsk, Russia

<sup>3</sup> University of Grenoble Alpes, CNRS UMR 5588, LIPhy, Grenoble F-38000, France

Number of pages: 22

22 November 2022

Number of tables: 4

Number of figures: 8

**Key words:** Nitrous oxide, N<sub>2</sub>O, CRDS, high resolution molecular spectroscopy, line parameters

\* Corresponding authors:

E-mails: alain.campargue@univ-grenoble-alpes.fr (A.Campargue), ekarlovets@gmail.com

(E.V.Karlovets)

**Abstract**

A high-sensitivity absorption spectrum of natural nitrous oxide has been recorded at 10 Torr between 8321 and 8620  $\text{cm}^{-1}$  (1.20 – 1.16  $\mu\text{m}$ ). The used cavity ring down spectrometer was referenced to a self-referenced frequency comb providing an accurate frequency scale of the spectra. The predictions of effective operator models were used for the line assignment. All identified bands correspond to the  $\Delta P=14-16$  series of transitions, where  $P=2V_1+V_2+4V_3$  is the polyad number ( $V_{i=1-3}$  are the vibrational quantum numbers). A total number of 3975 transitions belonging to the  $^{14}\text{N}_2^{16}\text{O}$ ,  $^{14}\text{N}^{15}\text{N}^{16}\text{O}$ ,  $^{15}\text{N}^{14}\text{N}^{16}\text{O}$ ,  $^{14}\text{N}_2^{18}\text{O}$ , and  $^{15}\text{N}_2^{16}\text{O}$  isotopologues were measured with estimated accuracy better  $1 \times 10^{-3} \text{ cm}^{-1}$  for most of the lines. Compared to the recent analysis of  $\text{N}_2\text{O}$  spectra at 1 Torr recorded in the same region (Karlovets et al. JQSRT, 262 (2021) 107508, doi: 10.1016/j.jqsrt.2021.107508), the higher pressure of the recordings and improved quality of the predictions have allowed to: (i) newly assign twenty-two bands, including the  $4\nu_3$  band of the  $^{15}\text{N}_2^{16}\text{O}$  minor isotopologue in natural isotopic abundance, (ii) extend the assignments of previously known bands, (iii) determine the small self-induced pressure shifts of the two strongest bands (less than  $10^{-4} \text{ cm}^{-1}$ ) by difference of the line positions at 1 and 10 Torr and use them to obtain the zero-pressure value of the line positions, (iv) derive new or improved spectroscopic constants of 69 bands from the standard band-by-band analysis, and (v) analyze six local resonance perturbations affecting three bands, including the identification of a few extra lines due to intensity transfer. Finally, the comparison of the line positions and intensities with their predicted values and with available databases is discussed.

## 1. Introduction

The analysis of the nitrous oxide room temperature spectra recorded at a pressure of 1 Torr using high sensitivity cavity ring down spectroscopy (CRDS) has been recently reported between 8325 and 8622  $\text{cm}^{-1}$  [1]. A total of 3305 lines belonging to 47 bands of the  $^{14}\text{N}_2^{16}\text{O}$ ,  $^{14}\text{N}^{15}\text{N}^{16}\text{O}$ ,  $^{15}\text{N}^{14}\text{N}^{16}\text{O}$ , and  $^{14}\text{N}_2^{18}\text{O}$  isotopologues were assigned. Among these bands, only the strongest five were previously measured (by Fourier transform spectroscopy) in the studied region. The assigned bands belong to the  $\Delta P=14-16$  series ( $P=2V_1+V_2+4V_3$  is the polyad number where  $V_i=1-3$  are the vibrational quantum numbers). Bands of the  $\Delta P=15$  series were reported for the first time. The line lists constructed in Ref. [1] for each  $\text{N}_2\text{O}$  isotopologue have allowed improving the predictions for the  $\Delta P=14-16$  series of transitions in the frame of the effective operator approach. The present work will benefit of these improved predictions (See below).

Here, we present a further step of the characterization of the nitrous oxide spectrum in the region based on newly recorded spectra at 10 Torr. The aim of this work is to extend and improve the rotational analysis of the previously observed bands and to reduce the fraction of unassigned lines (about 20% in Ref. [1]). As an illustration of the accuracy of the line center determination achieved by referencing the spectra to a self-referenced frequency comb, the small self-induced pressure shift of the two strongest bands (less than  $10^{-4} \text{ cm}^{-1}$ ) is presently determined by difference of the line positions at 1 and 10 Torr and used to obtain the zero-pressure value of the line positions (Section 3). In Section 4, we present the rovibrational assignments obtained by comparison with updated predictions based on the global modeling of the line positions and intensities performed within the framework of the method of effective operators. A total of 3975 transitions belonging to 69 bands of five  $\text{N}_2\text{O}$  isotopologues were rovibrationally assigned. Among the 69 measured bands, 22 are newly reported as for example the weak 0004e-0000e band of the  $^{15}\text{N}_2^{16}\text{O}$  isotopologue. The pressure-shift corrected values of the 10 Torr line positions measured in this work and of the 1 Torr positions values reported in Ref. [1] were used as input datasets of a fit providing accurate band-by-band spectroscopic constants. Six local perturbations are evidenced and analyzed in the region, including two interpolyad interactions.

## 2. Experimental set-up and line list construction

The spectra were recorded with the same setup as used in Ref. [1]. An external cavity diode laser (ECDL) was used to cover the 8321-8620  $\text{cm}^{-1}$  spectral region. The frequency calibration of the spectra uses a Fizeau type wavemeter and a self-referenced frequency comb, providing sub-100 kHz accuracy to the instantaneous frequency readings [2]. The reader is referred to Refs. [3-7] for the description of the cavity ring down spectrometer and the frequency tuning of the ECDL. The spectra were recorded in flow regime to decrease the impact of the lines of water vapor degassing from the cell walls. The flow of nitrous oxide (Alphagaz 99.99% stated purity) was roughly adjusted to 1 sccm

and the pressure was actively regulated at 10.00 Torr. The temperature of the outer wall of the stainless steel gas cell was continuously monitored evolved in the  $294.4 \pm 0.5$  K range.

The line centers and intensities were retrieved using an interactive least squares multi-lines fitting program written in LabVIEW software. The line profile was assumed to be of Voigt type. The line position, integrated absorbance, Lorentzian widths, and the corresponding local baseline (assumed to be a linear function of the wavenumber) were provided by the fitting procedure. The Gaussian component was fixed to the theoretical value of the Doppler width of the considered nitrous oxide isotopologue. **Fig. 2** illustrates the quality of the spectrum fit near  $8393 \text{ cm}^{-1}$ .

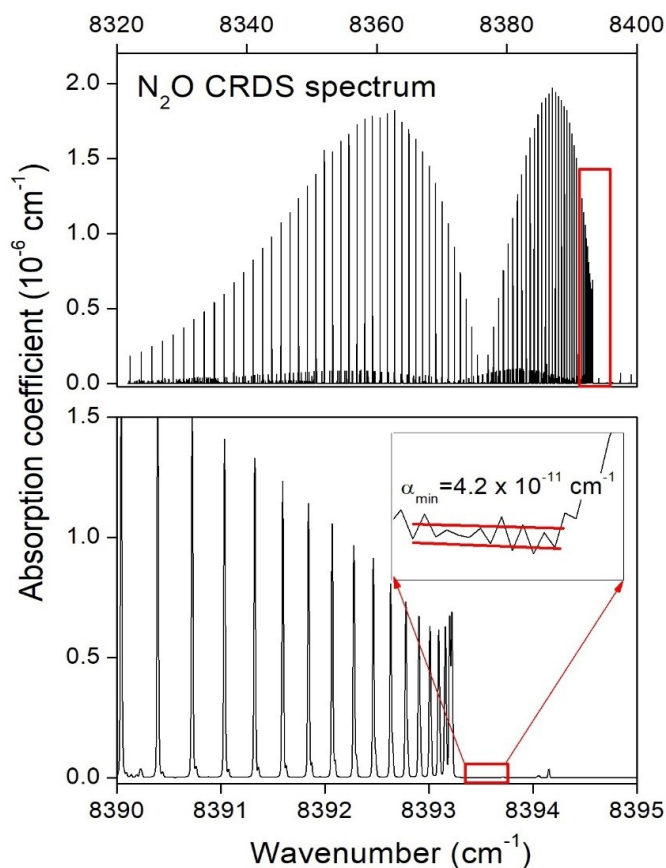


**Fig. 1.** CRDS spectrum of natural nitrous oxide between  $8390$  and  $8395 \text{ cm}^{-1}$  showing the *R* branch of the  $5001e-0000e$  ( $^{14}\text{N}_2^{16}\text{O}$ ) centred at  $8376.349 \text{ cm}^{-1}$ . The sample pressure was 10 Torr. Two successive enlargements show the typical achieved sensitivity: the noise level corresponding to the minimum value of the absorption coefficient which can be detected is about  $4.2 \times 10^{-11} \text{ cm}^{-1}$ .

Overall, the global lists include 5741 lines in the  $8321\text{--}8620 \text{ cm}^{-1}$  region. By comparison to the HITRAN spectroscopic database [8], 640 water lines were identified and removed from the list, leaving about 5100 lines to be rovibrationally assigned. We estimate that the accuracy of our measured line intensities to be 3% or better for most lines and up to 20% for the weakest or strongly blended lines.

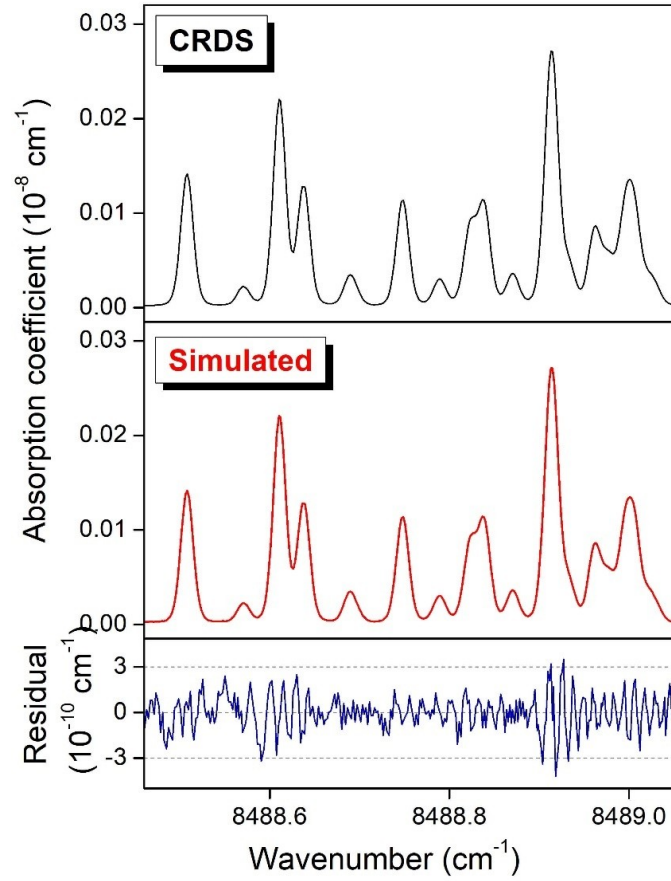


**Fig. 2.** Comparison of the CRDS spectrum of nitrous oxide in natural isotopic abundance recorded at 10 Torr with a simulation using a Voigt profile for each line. The residuals are displayed in the lower panel.

### 3. Self-induced pressure shift

The high signal to noise of the recorded spectra allows for a high precision in the line center determinations while the referencing to a frequency comb provides an accurate calibration of the frequency scale. As a result, highly accurate line centers could be derived from the spectra. The comparison of the position values at 1 Torr reported in Ref. [1] and the present values at 10 Torr shows that the accuracy of the measurement is sufficient to evidence the small ( $< 1 \times 10^{-4} \text{ cm}^{-1}$ ) shift of the line centers induced by the increase of the pressure from 1 to 10 Torr, at least in the case of the two strongest bands. **Fig. 3** presents the  $m$  dependence of the derived self-induced pressure shift for the 5001e-0000e and 3401e-0000e bands of  $^{14}\text{N}_2^{16}\text{O}$ . The measured differences were globally fitted by a straight line in the  $P$  and  $R$  branches, leading to the following self-induced pressure shift coefficients (in  $10^{-3} \text{ cm}^{-1}/\text{atm}$  unit):

$$-5.51(7) + 0.0892(41) \times m \quad (P \text{ branch}) \quad (1)$$

$$-5.18(12) - 0.1093(59) \times m \quad (R \text{ branch}) \quad (2)$$

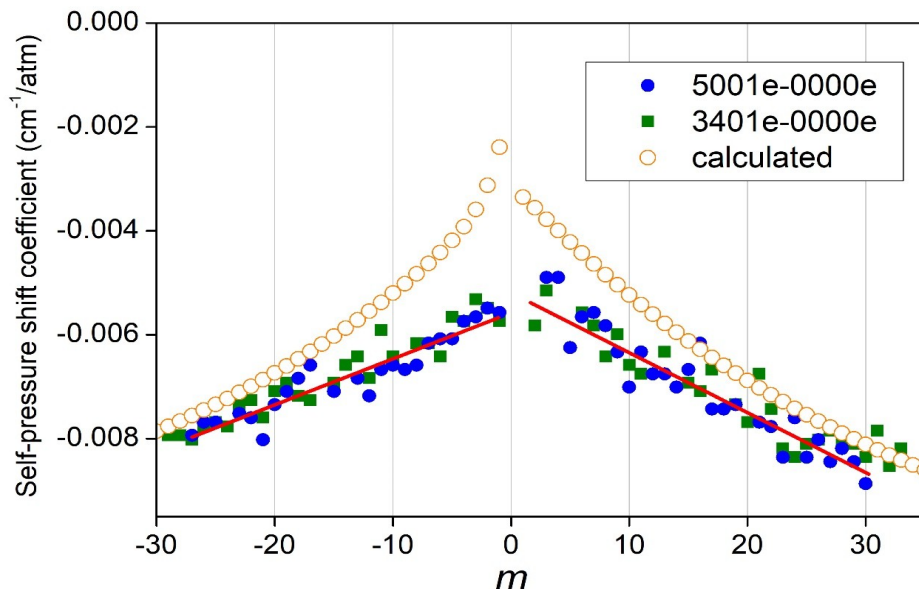


**Fig. 3.** Self-pressure shift coefficient of the 5001e-0000e and 3401e-0000e bands of  $^{14}\text{N}_2^{16}\text{O}$ , versus  $m$  ( $P$  branch:  $m=-J$ ,  $R$  branch:  $m=J+1$ ). The empirically calculated values of the two bands coincide [9] and are plotted for comparison (orange circles).

In a recent contribution, Hashemi et al. presented the update of the line-shape parameters of  $\text{N}_2\text{O}$  for the HITRAN2020 database [9]. Contrary, to the standard HITRAN line lists, the  $\text{N}_2\text{O}$  line list provided as Supplementary Material of Ref. [9], includes the self-pressure shift coefficients for the strong bands up to  $8000\text{ cm}^{-1}$ . These coefficients were empirically generated using literature measurements, following the method proposed by Hartmann [10]. The self-pressure shifts predicted for our 5001e-0000e and 3401e-0000e bands of interest are included in **Fig. 3**. In agreement with the measurements, the calculated values of the two bands coincide [this justifies our choice to fit globally the pressure shifts of the two bands (Eqs 1 and 2)]. The agreement with the measured values is good for high rotational levels but is less satisfactory for small ( $m$ ) values where the amplitude of the calculated values seem to be underestimated.

#### 4. Rovibrational analysis

##### 4.1. Assignment

The assignments were performed by comparison with predictions based on the effective operator approach. For  $^{14}\text{N}_2^{16}\text{O}$ , the non-polyad model of effective Hamiltonian (EH) [11] was used. The fitted values of the EH parameters were updated using the measurements of Ref.[1]. For  $^{14}\text{N}^{15}\text{N}^{16}\text{O}$ ,  $^{15}\text{N}^{14}\text{N}^{16}\text{O}$ ,  $^{14}\text{N}_2^{18}\text{O}$ , and  $^{15}\text{N}_2^{16}\text{O}$  the polyad models of Refs. [12-14] were used. The fitted values of the parameters of these models were also updated using the measurements of Ref. [1].

Line intensity calculations for a given isotopologue require both EH and effective dipole moment (EDM) models. EDM model depends on a set of the EDM parameters for each  $\Delta P$  value. The

computer code which was used for intensity calculations uses polyad models for EH and EDM. For  $^{14}\text{N}_2^{16}\text{O}$ , we used the EH model of Ref. [15], while the EH model of Ref. [13] was used for  $^{14}\text{N}^{15}\text{N}^{16}\text{O}$  and  $^{15}\text{N}^{14}\text{N}^{16}\text{O}$ . Finally, for  $^{14}\text{N}_2^{18}\text{O}$  and  $^{15}\text{N}_2^{16}\text{O}$  we used the EH models of Refs. [12,14]. The EDM model of Ref. [16] was used for all isotopologues.

**Table 1** summarizes the sources of the EH models and EDM parameters used to predict the spectrum of natural nitrous oxide in our region. For  $^{14}\text{N}_2^{16}\text{O}$ , the  $\Delta P= 14$  and 16 EDM parameters were fitted to measured intensity values of Refs [1,17-19]. The  $\Delta P= 15$  EDM parameters were newly determined using the first detected  $\Delta P= 15$  bands reported in Ref. [1]. In the case of the  $^{14}\text{N}^{15}\text{N}^{16}\text{O}$ ,  $^{15}\text{N}^{14}\text{N}^{16}\text{O}$ , and  $^{14}\text{N}_2^{18}\text{O}$  minor isotopologues, only  $\Delta P= 14$  and 16 bands were assigned and the corresponding EDM parameters were fitted using CRDS intensity values of Refs. [1,17]. Finally, the line intensities of the assigned  $\Delta P= 16$  band of  $^{14}\text{N}_2^{18}\text{O}$  were calculated using the corresponding EDM parameters of the main isotopologue. Global fits of the measured line intensities will be reported in separate papers.

**Table 1.** The references of the effective operator models used for the line position and intensity predictions of the five  $\text{N}_2\text{O}$  isotopologues.

Isotopologue	Line positions	Line intensities
$^{14}\text{N}_2^{16}\text{O}$	[11, 15]	$\Delta P= 14$ : [1,17-19] $\Delta P= 15$ : [1] $\Delta P= 16$ : [1,19]
$^{14}\text{N}^{15}\text{N}^{16}\text{O}$	[13]	$\Delta P= 14$ : [1,17] $\Delta P= 16$ : [1]
$^{15}\text{N}^{14}\text{N}^{16}\text{O}$	[13]	$\Delta P= 14$ : [1,17] $\Delta P= 16$ : [1]
$^{14}\text{N}_2^{18}\text{O}$	[12]	$\Delta P= 14$ : [1,17] $\Delta P= 16$ : [1,17]
$^{15}\text{N}_2^{16}\text{O}$	[14]	$\Delta P= 16$ : $^{14}\text{N}_2^{16}\text{O}$ EDM

Overall, 3134, 398, 315, 106, 22 transitions were assigned for the  $^{14}\text{N}_2^{16}\text{O}$ ,  $^{14}\text{N}^{15}\text{N}^{16}\text{O}$ ,  $^{15}\text{N}^{14}\text{N}^{16}\text{O}$ ,  $^{14}\text{N}_2^{18}\text{O}$ , and  $^{15}\text{N}_2^{16}\text{O}$  isotopologues, respectively. They belong to 69 vibrational bands of the  $\Delta P= 14$ -16 series of transitions. **Fig. 4** illustrates the difficulty of the line assignment on a  $1.2\text{ cm}^{-1}$  wide spectral region near  $8351\text{ cm}^{-1}$  where lines belonging to four  $\text{N}_2\text{O}$  isotopologues are observed. At the end of the assignment process, about 1120 lines, generally very weak (intensity less  $1.21 \times 10^{-30}$  cm/molecule) remained unassigned.

**Fig. 5** shows an overview comparison between the present CRDS observations and the predicted spectra for the five nitrous oxide isotopologues. The previous observations of Ref. [1] are highlighted for comparison. As a result of the higher pressure and higher quality of the predictions, twenty-two bands are newly reported compared to Ref. [1]- see also statistics in **Table 2**. They include the  $4\nu_3$  band of the  $^{15}\text{N}_2^{16}\text{O}$  isotopologue which has a relative abundance of only  $1.3 \times 10^{-5}$ .

The intensity values of the weakest lines are on the order of  $10^{-30}$  cm/molecule. The N<sub>2</sub>O assigned line list, provided as Supplementary Material I, includes the isotopologue identification, rovibrational assignments, line parameters observed in this work and predicted by the effective operator model. The line intensities of all nitrous oxide isotopologues are assumed to correspond to the natural abundance value included in **Table 2**.

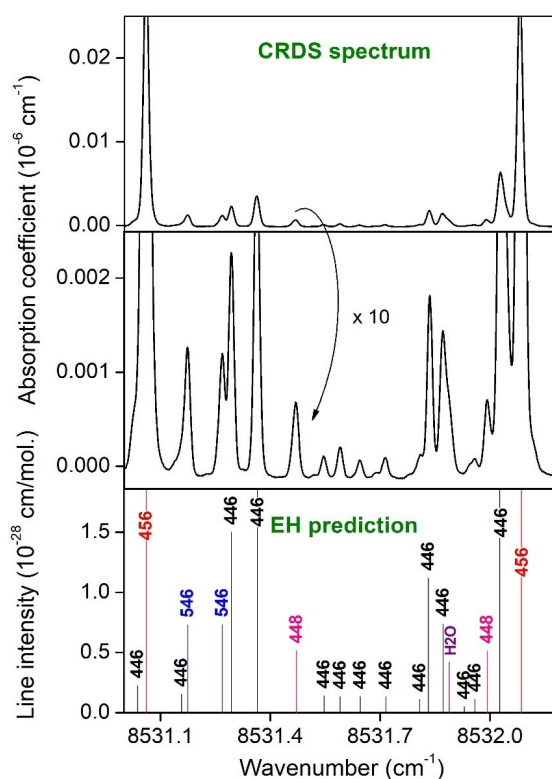


**Fig. 4.** The CRDS spectrum of natural nitrous oxide ( $P= 10$  Torr) between 8531 and 8532.2 cm<sup>-1</sup> (upper panel). The middle panel corresponds to an amplification factor of 10 for the ordinate scale. The stick spectra as predicted by the effective operator model are shown on the lower panel. Four N<sub>2</sub>O isotopologues contribute to the observed spectrum: 446 (<sup>14</sup>N<sub>2</sub><sup>16</sup>O), 456 (<sup>14</sup>N<sup>15</sup>N<sup>16</sup>O), 546 (<sup>15</sup>N<sup>14</sup>N<sup>16</sup>O), and 448 (<sup>14</sup>N<sub>2</sub><sup>18</sup>O).

**Table 2.** Number of transitions and bands assigned in this work and in Ref. [1] between 8321 and 8620 cm<sup>-1</sup>

Molecule	Abundance	Number of transitions <i>a</i>	Number of bands <i>a</i>
<sup>14</sup> N <sub>2</sub> <sup>16</sup> O	0099033 [8]	3134 (389)	53 (14)
<sup>14</sup> N <sup>15</sup> N <sup>16</sup> O	0.003641 [8]	398 (99)	6 (3)
<sup>15</sup> N <sup>14</sup> N <sup>16</sup> O	0.003641 [8]	315 (116)	6 (3)
<sup>14</sup> N <sub>2</sub> <sup>18</sup> O	0.001986 [8]	106 (42)	3 (2)
<sup>15</sup> N <sub>2</sub> <sup>16</sup> O	$1.33857 \times 10^{-5}$	22 (22)	1 (1)
<b>Total</b>	<b>1</b>	<b>3975 (668)</b>	<b>69 (23)</b>

*Note*

<sup>a</sup> Numbers in parenthesis correspond to new transitions or bands compared to Ref. [1];

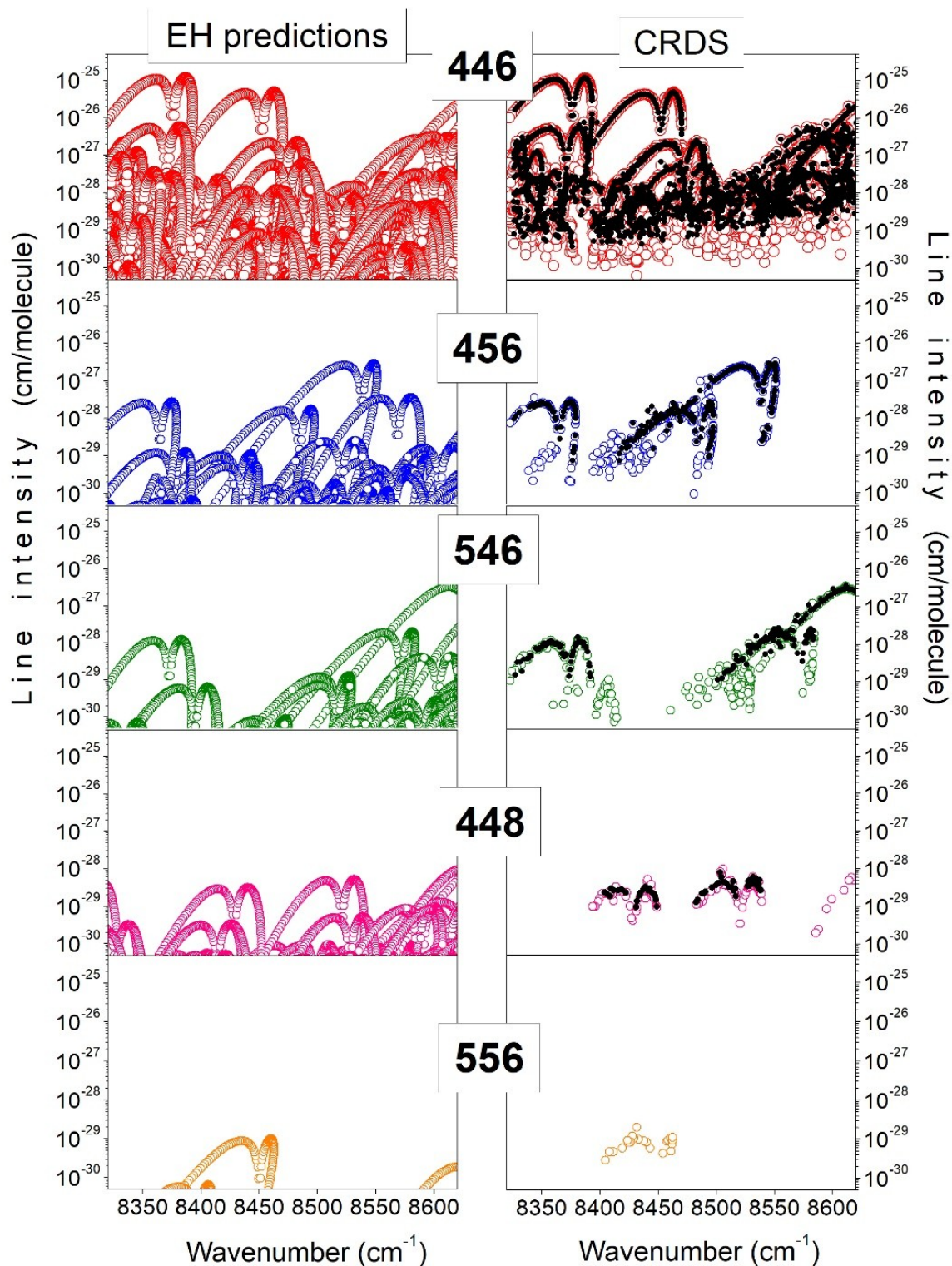


**Fig. 5.** Overview comparison between the transitions of  $^{14}\text{N}_2^{16}\text{O}$  (446),  $^{14}\text{N}^{15}\text{N}^{16}\text{O}$  (456),  $^{15}\text{N}^{14}\text{N}^{16}\text{O}$  (546),  $^{14}\text{N}_2^{18}\text{O}$  (448), and  $^{15}\text{N}_2^{16}\text{O}$  (556) assigned in the CRDS spectrum of nitrous oxide in natural isotopic abundance between 8321 and 8620  $\text{cm}^{-1}$  (right panels) and the corresponding spectra predicted in the frame of the effective operator approach (left panels). Previous measurements of Ref. [1] are highlighted for comparison (black dots).

**Fig 6** shows the residuals between the measured and EH predicted line positions. The comparison is provided both with the line positions at 10 Torr obtained in this work and with recently

measured at 1 Torr in Ref. [1]. The refinement of the EH parameters by using the 1 Torr positions of Ref. [1] have allowed to reduce part of the deviations and the obtained agreement illustrates the very good predictive ability of the EH model. For the  $^{14}\text{N}_2^{16}\text{O}$  isotopologue, the root mean square (RMS) values of the  $(\nu_{\text{obs}} - \nu_{\text{EH}})$  deviations is  $0.02 \text{ cm}^{-1}$ . Future inclusion of the new observations as input data in the fit of the EH parameters will further help to improve the set of EH parameters of the five isotopologues.

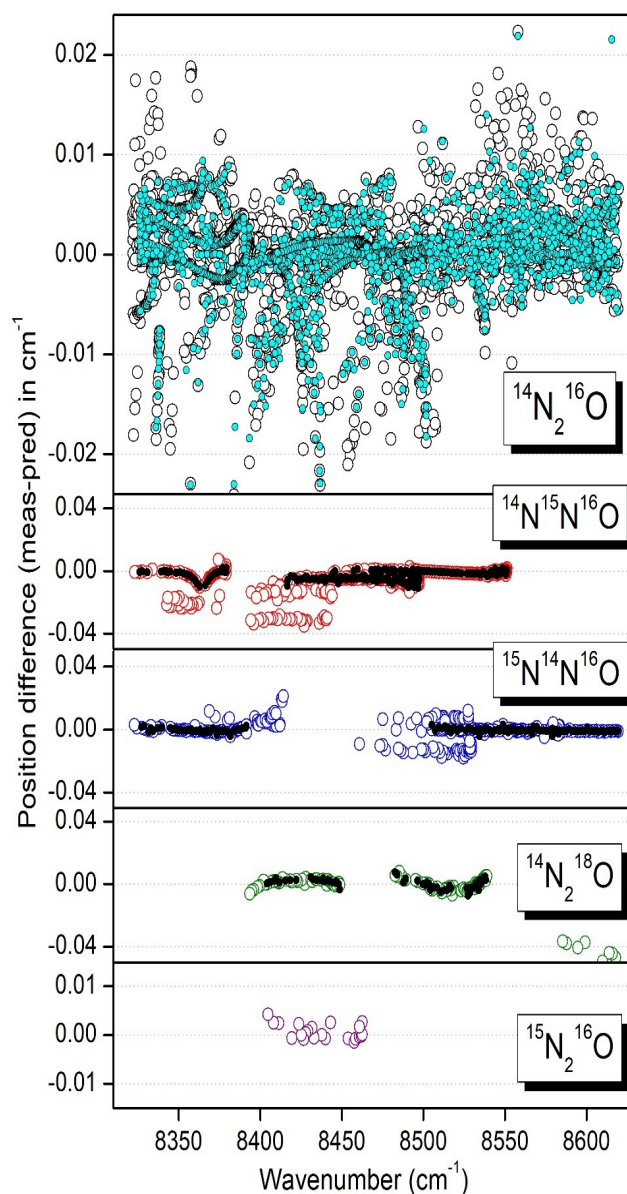


**Fig. 6.** Differences between the line positions predicted using the effective Hamiltonians and the measured CRDS values at 10 Torr (open circles) and at 1 Torr (filled circles) for the five  $\text{N}_2\text{O}$  isotopologues.

#### 4.2. Band-by-band rotational analysis

The extension of the rotational assignments for most of the previously reported bands and the newly assigned bands made suitable a new fit of the spectroscopic parameter values for all the

observed bands. Line positions of all the bands were corrected from the small self-induced pressure shifts using the empirical law determined above (Eqs 1 and 2). When available, the 1 Torr position values of Ref. [1] were gathered with the presently measured 10 Torr positions. The band-by-band spectroscopic constants were derived from a fit of the resulting dataset using the standard expression of the vibration-rotational energy levels:

$$F_v(J) = G_v + B_v J(J+1) - D_v J^2(J+1)^2 + H_v J^3(J+1)^3 \quad (3)$$

where  $G_v$  is the vibrational term value,  $B_v$  is the rotational constant,  $D_v$  and  $H_v$  are the centrifugal distortion constants,  $J$  is the angular momentum quantum number. The spectroscopic parameters were fitted directly to the observed wavenumbers and, in the case of hot bands involving  $e$  and  $f$  rotational levels, the  $ee$ ,  $ef$ ,  $fe$ , and  $ff$  sub-bands were considered independently. The lower state constants were constrained to their literature values obtained by Toth [18,20] or obtained from a global simultaneous fit of the lower and upper state constants. Overall, rovibrational parameter values of 68 bands of five  $N_2O$  isotopologues were determined. They are listed in **Table 3** in increasing value of band center. For completeness, we have included in the Table the  $4\nu_3$  band of the  $^{14}N_2^{18}O$  isotopologue although the fit of spectroscopic parameters was not possible because of too reduced input data set. We provide only the band center predicted by the global effective Hamiltonian for this band.

Excluding a few outliers, the *rms* values of the (meas. – calc.) position differences of the unperturbed bands range between  $2.8 \times 10^{-4} \text{ cm}^{-1}$  and  $9.9 \times 10^{-4} \text{ cm}^{-1}$ . The results of the fit are given as Supplementary Material II. This archive file includes for each band, the spectroscopic parameters of the lower state fixed to the literature values (except those of the 0420 and 0440 lower states of  $^{14}N_2^{16}O$  which were fitted), fitted spectroscopic parameters of the upper state, errors on the fitted parameters (in % and in  $\text{cm}^{-1}$ ) and measured and calculated line positions.

#### 4.3. Rovibrational perturbations

Among the 69 analyzed bands, four  $^{14}N_2^{16}O$  bands were found to be affected by local resonance perturbations. Two of them were reported in Ref. [1]. The interaction mechanism and interacting levels were identified based on the effective Hamiltonian model. **Table 4** lists the bands affected by resonance interaction together with the interaction mechanism, the  $J$  value corresponding to the energy crossing and their band centers. **Fig. 7** illustrates the shift of the energy levels from their unperturbed values evaluated using the spectroscopic parameters (Eq. 3 and Table 4).

**Table 4.** Summary of the local resonance interactions of the  $^{14}N_2^{16}O$  bands evidenced between 8321 and  $8620 \text{ cm}^{-1}$

Perturbed band	Center ( $\text{cm}^{-1}$ )	Upper state ( $P \ I_2 \ i$ )	Resonance interaction mechanism	$J_{cros}$ <i>s</i>
----------------	-----------------------------	-------------------------------	---------------------------------	------------------------

6001e-1000e	8321.42984	(16 0 19)	Intrapolyad anharmonic interaction (16 0 19) $\leftrightarrow$ (16 0 18)	29
1004e-1000e	8603.66282	(18 0 4)	Intrapolyad anharmonic interaction (18 0 4) $\leftrightarrow$ (18 0 3)	14
			Interpolyad Coriolis interaction (18 0 4) $\leftrightarrow$ (17 1 10)	34
			Interpolyad anharmonic interaction (18 0 4) $\leftrightarrow$ (16 0 22)	45
3401e-0000e	8452.63588	(14 0 15)	Interpolyad Coriolis interaction (14 0 15) $\leftrightarrow$ (15 3 23)	51
0224e-0220e	8600.95864	(18 2 2)	Interpolyad anharmonic interaction (18 2 2) $\leftrightarrow$ (16 2 38)	47

Let us recall that the N<sub>2</sub>O vibrational levels are grouped in polyads of strongly interacting states gathering states with the same polyad number  $P = 2V_1 + V_2 + 4V_3$ . In addition, to the usual  $V_1 V_2 V_3$  labeling corresponding to the maximum value of the modulo of the expansion coefficients of the eigenfunctions, the cluster labelling notation,  $(P, l_2, i)$ , is also conveniently used ( $i$  is the order number within the cluster increasing with the energy). Up to recently, only polyad model of the N<sub>2</sub>O effective Hamiltonians were available thus neglecting inter-polyad coupling mechanisms. The non-polyad model of the effective Hamiltonian recently developed for the main isotopologue [11], takes into account three types of interpolyad interactions (in particular Coriolis interaction) allowing for  $\Delta P = 1$  or 2 couplings. Among the six evidenced perturbations, three are inter-polyad perturbations.

**Fig. 7a** shows the effect of the anharmonic resonance interaction between the 6001e and 0(16)00e states belonging to the  $P = 16$  polyad, *versus* the  $J$  rotational quantum number. This perturbation was previously evidenced in Ref. [1]. Here, we could assign twelve extra lines resulting from an intensity transfer from the 6001e-1000e band to the 0(16)00e-1000e band. Note that a few of these assignments are supported by lower state combination relations between  $P(J+1)$  and  $R(J-1)$  extra lines. Let us mention that the P29-P31, P33, and P36 extra lines fall below the range of the present recordings ( $8321\text{--}8620\text{ cm}^{-1}$ ) and were identified among the unassigned lines of Ref. [17]. The 6001e-1000e line positions measured in Refs [1,17] and in this work were included in the fit of the spectroscopic constants whereas the perturbed lines were excluded from the fit.

A second perturbed band is the 1004e-1000e of <sup>14</sup>N<sub>2</sub><sup>16</sup>O at  $8603.7\text{ cm}^{-1}$  reaching the (18 0 4) upper state (**Fig. 7b**) which is affected by both a  $\Delta P = 0$  intra-polyad perturbation and  $\Delta P = 1$  and 2 inter-polyad perturbations. Compared to Ref. [1], the  $\Delta P = 2$  interpolyad anharmonic interaction between (18 0 4) and (16 0 22) vibrational states around  $J = 45$  is newly evidenced and two extra lines (P36 and R34) of the 3312e-1000e perturbing band could be unambiguously assigned.

The intra-polyad perturbations affecting high  $J$  values of the 3401e and 0224e [(14 0 15) and (18 2 2) in triplet notation, respectively] states are newly reported (**Fig. 7c and 7d**, respectively). The

shift of the perturbed line positions reaches about  $10^{-2} \text{ cm}^{-1}$  around the energy crossing at  $J= 51$  and  $J= 47$ , respectively.

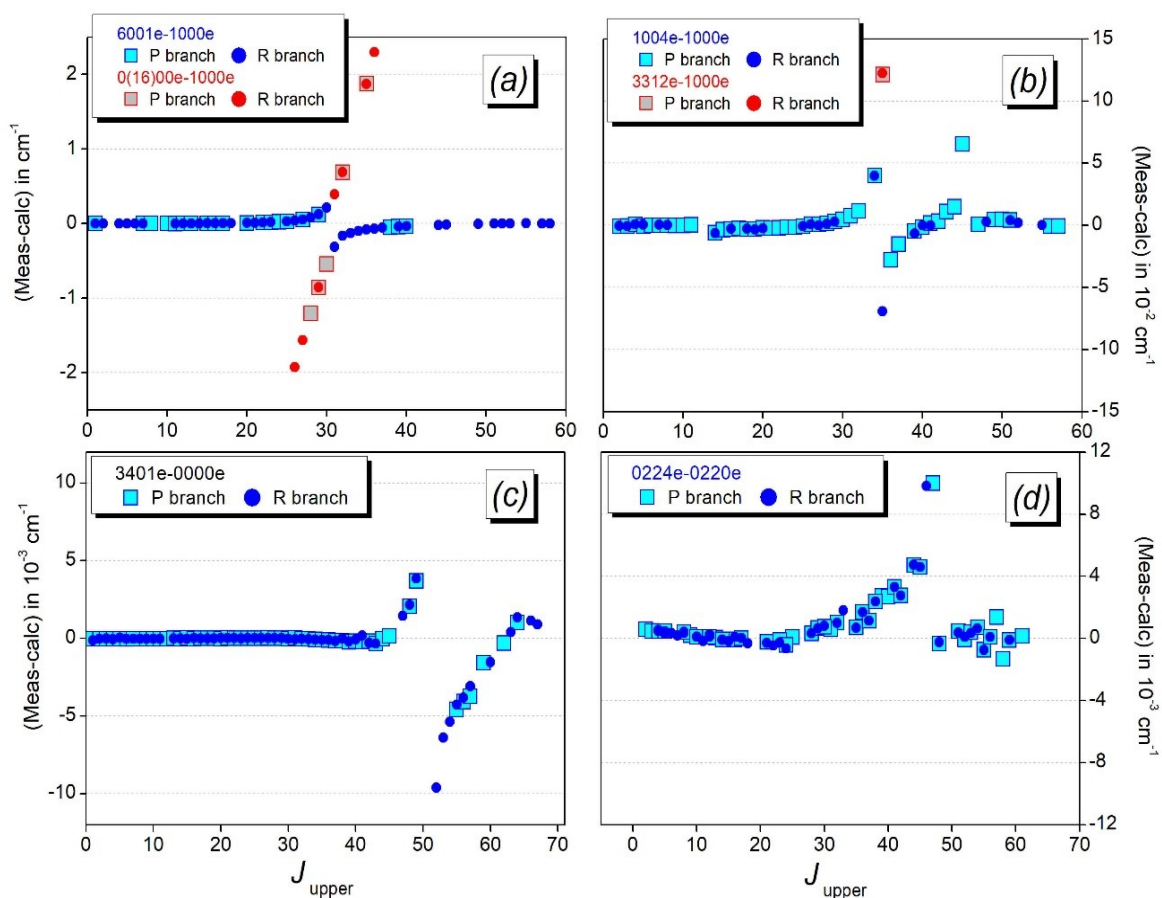


**Fig. 7.** Residuals between the unperturbed line positions calculated with the fitted values of the spectroscopic parameters (see Eq. (3)) and the values measured by CRDS, versus the  $J$  rotational quantum number:

**(a)** Intrapolyad anharmonic resonance interaction between 6001e ( $P= 16$ ) and 0(16)00e ( $P= 16$ ) vibrational states of  $^{14}\text{N}_2^{16}\text{O}$  isotopologue (energy levels crossing at  $J= 29$ );

**(b)** Intrapolyad anharmonic resonance interaction between 1004e ( $P= 18$ ) and 1802e ( $P= 18$ ) states (energy levels crossing at  $J= 14$ ); 2) Interpolyad Coriolis interaction between 1004e ( $P= 18$ ) and 3312e ( $P= 17$ ) (energy levels crossing at  $J= 34$ ); 3) Interpolyad anharmonic resonance interaction between 1004e ( $P= 18$ ) and 8000e ( $P= 16$ ) states (energy levels crossing at  $J= 45$ );

**(c)** Interpolyad Coriolis interaction between 3401e ( $P= 14$ ) and 2332e ( $P= 15$ ) (energy levels crossing at  $J= 51$ );

**(d)** Interpolyad anharmonic interaction between 0224e ( $P= 18$ ) and 7220e ( $P= 16$ ) vibrational states (energy levels crossing at  $J= 47$ ).

## 5. Conclusion

New recordings by cavity ring down spectroscopy referenced to a self-referenced frequency comb have allowed to improve the characterization of the absorption spectrum of nitrous oxide in the 1.20 – 1.16  $\mu\text{m}$  region. Compared to the spectra at 1 Torr of Ref. [1], the 10 Torr pressure of the present recordings allowed lowering the sensitivity threshold by a factor of about ten and lines with intensity on the order of  $10^{-30}$  have been measured (see Fig. 5). These spectra combined with

improved predictions based on effective operator models were used to extend the assignments and identifying twenty-two new bands. The small self-induced pressure shifts of the two strongest bands have been determined by difference of the line positions at 1 and 10 Torr. The resulting set of line positions was corrected at zero-pressure value and used to determine the band-by-band spectroscopic constants.

A detailed discussion of the HITRAN2016 and HITEMP line lists in the region has been included in Ref. [1] (Note that the Nitrous Oxide Spectroscopy Databank (NOSD) [21] does not extend beyond  $8310\text{ cm}^{-1}$ ). The HITRAN2020 line list [22] in the near infrared is unchanged compared to HITRAN2016 and the total absence of  $^{14}\text{N}_2^{16}\text{O}$  data in our region remains. The recent HITEMP list [23] was computed using the effective operator approach in a similar way as NOSD but extends up to  $10500\text{ cm}^{-1}$ . As discussed in Ref. [1], the HITEMP list in our region is incomplete (it includes only 31 bands of  $^{14}\text{N}_2^{16}\text{O}$  and 4 bands of  $^{14}\text{N}_2^{18}\text{O}$  compared to 69 bands presently reported). In particular, the  $\Delta P=15$  bands are totally missing because the corresponding EDM parameters were unknown.

We present in **Fig. 8** an overview of the spectral intervals covered by our different CRDS investigation within the last fifteen years. They cover the  $5696\text{-}8630\text{ cm}^{-1}$  range and provide the main source of line positions used to refine the parameters of the  $\text{N}_2\text{O}$  EH models [11-15]. The HITEMP and HITRAN lists of  $^{14}\text{N}_2^{16}\text{O}$  are included in the plot. The HITRAN list corresponds to an intensity cut off of  $2\times 10^{-25}\text{ cm}^2/\text{molecule}$  at 296 K i.e. about 4-5 orders of magnitude above the CRDS detectivity threshold. Up to now the EDM parameters used to generate the NOSD and HITEMP databases benefited only partly from the CRDS studies. Indeed, as highlighted on **Fig. 8**, line intensities were retrieved for only part of the recorded CRDS spectra. Consequently, as it is the case in the present region, the HITEMP [23] or NOSD [21] line lists show a fraction of bands with underestimated intensities or missing, because of undetermined EDM parameters (*e.g.*  $\Delta P=15$  bands). These bands are generally weak at room temperature but, as they include mostly hot bands, their impact is expected to increase at higher temperature. In the future, we plan to derive accurate line intensities in the CRDS regions missing intensity information and construct an empirical database of natural nitrous oxide in the  $5696\text{-}8630\text{ cm}^{-1}$  range with an intensity cut off on the order of  $10^{-29}\text{ cm}^2/\text{molecule}$ .

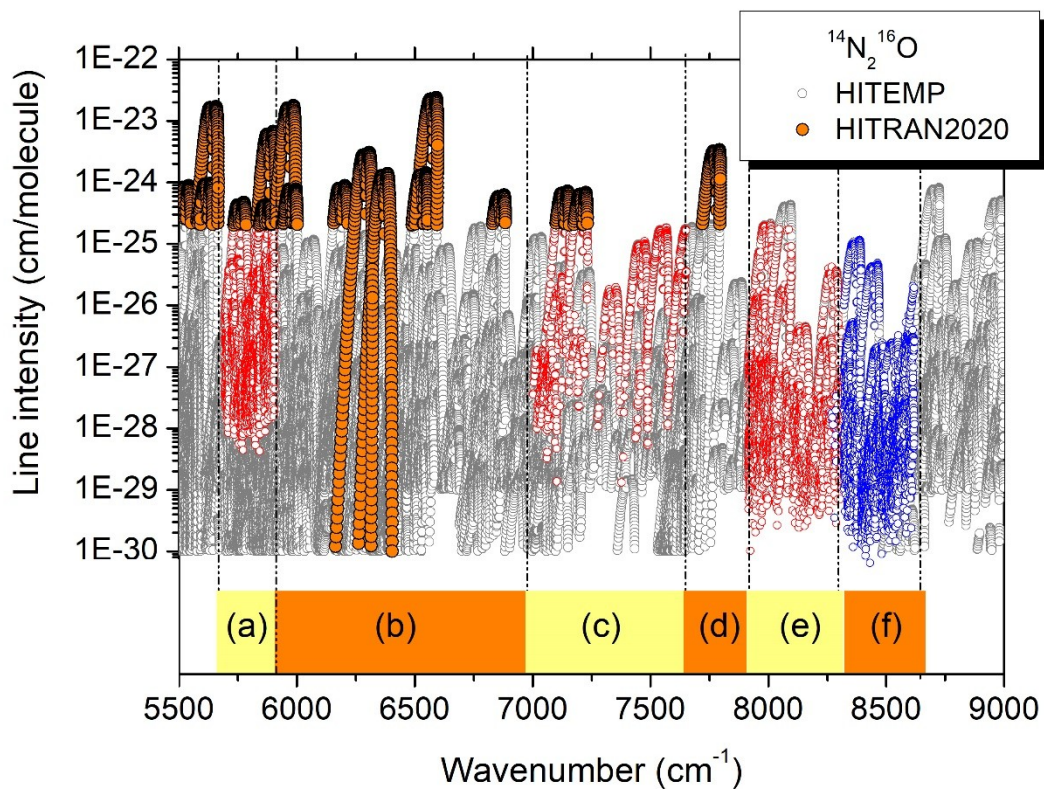


**Fig. 9.** Overview of the HITEMP and HITRAN line lists of  $^{14}\text{N}_2^{16}\text{O}$  between 5500 and 9000  $\text{cm}^{-1}$  (grey and orange symbols, respectively). The range of previous CRDS investigations is indicated: (a): 5696-5910  $\text{cm}^{-1}$  [24], (b) 5905-7066  $\text{cm}^{-1}$  [25-27], (c) 6950-7653  $\text{cm}^{-1}$  [28,29], (d) 7647-7918  $\text{cm}^{-1}$  [30], (e):7915-8334  $\text{cm}^{-1}$  [12,17], (f): 8320-8622  $\text{cm}^{-1}$  [1] and this work. Red and blue circles correspond to CRDS intensity measured in previous studies and in this work, respectively.

#### Acknowledgements

We thank Robab Hashemi (Harvard-Smithsonian Center for Astrophysics, Cambridge, USA) for the calculations of the self-pressure shifts included in Figure 3. This work is supported by CNRS (France) in the frame of the International Research Project "SAMIA" with IAO-Tomsk.

## References

1. Karlovets EV, Kassi S, Tashkun SA, Campargue A. The absorption spectrum of nitrous oxide between 8325 and 8622  $\text{cm}^{-1}$ . *J Quant Spectrosc Radiat Transfer* 2021;262:107508. <https://doi.org/10.1016/j.jqsrt.2021.107508>.
2. Kassi S, Stoltmann T, Casado M, Daëron M, Campargue A. Lamb dip CRDS of highly saturated transitions of water near 1.4  $\mu\text{m}$ . *J Chem Phys* 2018;148:054201. <https://doi.org/10.1063/1.5010957>.
3. Mondelain D, Kassi S, Sala T, Romanini D, Marangoni M, Campargue A. Sub-MHz accuracy measurement of the S(2) 2–0 transition frequency of  $\text{D}_2$  by comb-assisted cavity ring down spectroscopy. *J Mol Spectrosc* 2016; 326:5–8. <https://doi.org/10.1016/j.jms.2016.02.008>.
4. Kassi S, Campargue A. Cavity Ring Down Spectroscopy with  $5 \times 10^{-13} \text{ cm}^{-1}$  sensitivity. *J Chem Phys* 2012; 137:234201. <https://doi.org/10.1063/1.4769974>.
5. Konefał M, Mondelain D, Kassi S, Campargue A. High sensitivity spectroscopy of the  $\text{O}_2$  band at 1.27  $\mu\text{m}$ : (I) pure  $\text{O}_2$  line parameters above 7920  $\text{cm}^{-1}$ . *J Quant Spectrosc Radiat Transfer* 2020; 241:106653. <https://doi.org/10.1016/j.jqsrt.2019.106653>.
6. Mondelain D, Mikhailenko SN, Karlovets EV, Béguier S, Kassi S, Campargue A. Comb-Assisted Cavity Ring Down Spectroscopy of  $^{17}\text{O}$  enriched water between 7443 and 7921  $\text{cm}^{-1}$ . *J Quant Spectrosc Radiat Transfer* 2017; 203:206–12. <https://doi.org/10.1016/j.jqsrt.2017.03.029>.
7. Kassi S, Stoltmann T, Casado M, Daëron M, Campargue A. Lamb dip CRDS of highly saturated transitions of water near 1.4  $\mu\text{m}$ . *J Chem Phys* 2018; 148:054201. <https://doi.org/10.1063/1.5010957>.
8. Gordon IE, Rothman LS, Hill C, Kochanov RV, Tan Y, Bernath PF, et al. The HITRAN2016 molecular spectroscopic database. *J Quant Spectrosc Radiat Transfer* 2017; 203:3–69. <https://doi.org/10.1016/j.jqsrt.2017.06.038>.
9. Hashemi R, Gordon IE, Adkins EM, Hodjes JT, Long DA, Birk M, Loos J, et al. Improvement of the spectroscopic parameters of the air- and self-broadened  $\text{N}_2\text{O}$  and  $\text{CO}$  lines for the HITRAN2020 database applications. *J Quant Spectrosc Radiat Transfer* 2021; 271:107735. <https://doi.org/10.1016/j.jqsrt.2021.107735>.
10. Hartmann J-M. A simple empirical model for the collisional spectral shift of air-broadened  $\text{CO}_2$  lines. *J Quant Spectrosc Radiat Transf* 2009;110(18):2019–26. <https://doi.org/10.1016/j.jqsrt.2009.05.016>.
11. Tashkun SA. Global modeling of the  $^{14}\text{N}_2^{16}\text{O}$  line positions within the framework of the non-polyad model of effective Hamiltonian. *J Quant Spectrosc Radiat Transfer* 2019; 231:88–101. <https://doi.org/10.1016/j.jqsrt.2019.04.023>.
12. Tashkun SA, Perevalov VI, Karlovets EV, Kassi S, Campargue A. High sensitivity Cavity Ring Down Spectroscopy of  $\text{N}_2\text{O}$  near 1.22  $\mu\text{m}$ : (II)  $^{14}\text{N}_2^{16}\text{O}$  line intensity modeling and global fit of  $^{14}\text{N}_2^{18}\text{O}$  line positions. *J Quant Spectrosc Radiat Transfer* 2016; 176:62–9. <https://doi.org/10.1016/j.jqsrt.2016.02.020>.
13. Tashkun SA, Perevalov VI, Kochanov RV, Liu AW, Hu SM. Global fitting of  $^{14}\text{N}^{15}\text{N}^{16}\text{O}$  and  $^{15}\text{N}^{14}\text{N}^{16}\text{O}$  vibrational-rotational line positions using the effective Hamiltonian approach. *J Quant Spectrosc Radiat Transfer* 2010;111(9):1089–1105. <https://doi.org/10.1016/j.jqsrt.2010.01.010>.
14. Tashkun SA, Perevalov VI, Liu AW, Hu SM. Global modeling of the  $^{15}\text{N}_2^{16}\text{O}$  line positions within the framework of the polyad model of effective Hamiltonian and a room temperature  $^{15}\text{N}_2^{16}\text{O}$  line list. *J Quant Spectrosc Radiat Transfer* 2016;175:1–7. <https://doi.org/10.1016/j.jqsrt.2016.01.038>.
15. Perevalov VI, Tashkun SA, Kochanov RV, Liu AW, Campargue A. Global modeling of the  $^{14}\text{N}_2^{16}\text{O}$  line positions within the framework of the polyad model of effective Hamiltonian. *J Quant Spectrosc Radiat Transfer* 2012; 113:1004–12. <https://doi.org/10.1016/j.jqsrt.2011.12.008>.
16. Lyulin OM, Perevalov VI, Teffo JL. Effective dipole moment and band intensities of nitrous

- oxide. *J Mol Spectrosc* 1995; 174:566–80. <https://doi.org/10.1006/jmsp.2000.8269>.
17. Karlovets EV, Campargue A, Kassi S, Perevalov VI, Tashkun SA. High sensitivity Cavity Ring Down Spectroscopy of N<sub>2</sub>O near 1.22 μm: (I) Rovibrational assignments and band-by-band analysis. *J Quant Spectrosc Radiat Transfer* 2016;169:36–48. <https://doi.org/10.1016/j.jqsrt.2015.09.012>.
  18. Toth RA. Line Positions and Strengths of N<sub>2</sub>O between 3515 and 7800 cm<sup>-1</sup>. *Journal of Molecular Spectroscopy* 1999; 197:158–87. <https://doi.org/10.1006/jmsp.1999.7907>.
  19. Daumont L, Auwera JV, Teffo JL, Perevalov VI, Tashkun SA. Line intensity measurements in <sup>14</sup>N<sub>2</sub><sup>16</sup>O and their treatment using the effective dipole moment approach. II. The 5400–11000 cm<sup>-1</sup> region. *J Quant Spectrosc Radiat Transfer* 2007;104(3):342–356. <https://doi.org/10.1016/j.jqsrt.2006.09.004>.
  20. Toth RA. Linelist of N<sub>2</sub>O parameters from 500 to 7500 cm<sup>-1</sup>. <http://mark4sun.jpl.nasa.gov/n2o.html>.
  21. Tashkun SA, Perevalov VI, Lavrentieva NN. NOD-1000, the high-temperature nitrous oxide spectroscopic databank. *J Quant Spectrosc Radiat Transfer* 2016; 177:43–8. <https://doi.org/10.1016/j.jqsrt.2015.11.014>.
  22. Gordon IE, Rothman LS, Hargreaves RJ, Hashemi R, Karlovets EV, Skinner FM, et al. The HITRAN2020 molecular spectroscopic database. *J Quant Spectrosc Radiat Transfer* 2021, in press. <https://doi.org/10.1016/j.jqsrt.2021.107949>.
  23. Hargreaves RJ, Gordon IE, Rothman LS, Tashkun SA, Perevalov VI, Lukashetskaya AA, et al. Spectroscopic line parameters of NO, NO<sub>2</sub>, and N<sub>2</sub>O for the HITEMP database. *J Quant Spectrosc Radiat Transfer* 2019; 232:35–53. <https://doi.org/10.1016/j.jqsrt.2019.04.040>.
  24. Bertin T, Mondelain D, Karlovets EV, Kassi S, Perevalov VI, Campargue A. High sensitivity cavity ring down spectroscopy of N<sub>2</sub>O near 1.74 μm. *J Quant Spectrosc Radiat Transfer* 2019;229:40–9. <https://doi.org/10.1016/j.jqsrt.2019.02.011>.
  25. Liu AW, Kassi S, Malara P, Romanini D, Perevalov VI, Tashkun SA, Hu SM, Campargue A. High sensitivity CW-cavity ring down spectroscopy of N<sub>2</sub>O near 1.5 μm (I). *J Mol Spectrosc* 2007;244;33–47. <https://doi.org/10.1016/j.jms.2006.03.007>.
  26. Liu AW, Kassi S, Perevalov VI, Tashkun SA, Campargue A. High sensitivity CW-cavity ring down spectroscopy of N<sub>2</sub>O near 1.5 μm (II). *J Mol Spectrosc* 2007;244;48–62. <https://doi.org/10.1016/j.jms.2007.05.010>.
  27. Liu AW, Kassi S, Perevalov VI, Hu SM, Campargue A. High sensitivity CW-cavity ring down spectroscopy of N<sub>2</sub>O near 1.5 μm (III). *J Mol Spectrosc* 2009; 254:20–7. <https://doi.org/10.1016/j.jqsrt.2019.02.011>.
  28. Lu Y, Mondelain D, Liu AW, Perevalov VI, Kassi S, Campargue A. High Sensitivity CW-Cavity Ring Down Spectroscopy of N<sub>2</sub>O between 6950 and 7653 cm<sup>-1</sup> (1.44–1.31 μm): I. Line positions. *J Quant Spectrosc Radiat Transfer* 2012; 113:749–62. <https://doi.org/10.1016/j.jqsrt.2012.03.005>.
  29. Karlovets EV, Lu Y, Mondelain D, Kassi S, Campargue, Tashkun SA, Perevalov VI, High sensitivity CW-Cavity Ring Down Spectroscopy of N<sub>2</sub>O between 6950 and 7653 cm<sup>-1</sup> (1.44–1.31 μm): II. Line intensities. *J Quant Spectrosc Radiat Transfer* 2013; 117:81–7. <https://doi.org/10.1016/j.jqsrt.2012.11.003>.
  30. Liu AW, Kassi S, Perevalov VI, Tashkun SA, Campargue A. High sensitivity CW-cavity ring down spectroscopy of N<sub>2</sub>O near 1.28 μm. *J Mol Spectrosc* 2011;267;191–9. <https://doi.org/10.1016/j.jms.2011.03.025>.

**Table 3.** Spectroscopic parameters (in  $\text{cm}^{-1}$ ) for the different bands of  $\text{N}_2\text{O}$  isotopologues assigned in the CRDS spectrum between 8321 and 8620  $\text{cm}^{-1}$ .

Band <sup>a</sup>	$(P\ l_2\ i)^b$	$\Delta G_v^c$	$G_v$	$B_v$	$D_v \times 10^7$	$H_v \times 10^{12}$	$RMS_d$	$N_{fit}/N_{obs}^e$	$J_{max\ P/Q/R}^f$	$\Delta P_g$	Note <sup>h</sup>
<b><sup>14</sup>N<sub>2</sub><sup>16</sup>O isotopologue</b>											
6111e-1110e	(17 1 17)-(3 1 2)	8316.47857(59)	10196.74431(59)	0.4073122(43)	0.503(60)	-	0.81	18/25	P9/R24	14	1,2
6111f-1110f		8316.47619(32)	10196.74194(32)	0.4096967(19)	1.363(26)	7.77(92)	0.65	28/39	P14/R44	14	1,2
0(10)01e-0000e	(14 0 13)-(0 0 1)	8319.79327(22)	8319.79327(22)	0.4178033(16)	12.879(26)	156.7(11)	0.72	61/68	P23/R39	14	1,2
6001e-1000e	(16 0 19)-(2 0 2)	8321.42984(32)	9606.33318(32)	0.4072611(25)	1.780(16)	15.11(10)	0.90	30/66	P41/R57	14	1,3
1113e-0000e	(15 1 3)-(0 0 1)	8335.796703(62)	8335.796703(62)	0.40719707(12)	1.70914(39)	-	0.41	118/121	P14/R61	15	2
1113f-0000e		8335.796309(71)	8335.796309(71)	0.40804139(35)	1.6950(32)	-	0.28	58/60	Q35	15	2
6111e-0310e	(17 1 17)-(3 1 1)	8338.13327(25)	10087.19849(25)	0.40871016(92)	2.2704(57)	-	0.77	30/39	P14/R42	14	2
6111f-0310f		8338.13276(21)	10087.19791(21)	0.4113417(10)	2.5040(84)	-	0.61	28/36	P16/R36	14	2
6001e-0200e	(16 0 17)-(2 0 1)	8349.74197(12)	9517.87427(12)	0.4094582(17)	3.543(56)	20.6(45)	0.49	82/88	P25/R28	14	2
5331e-0330e	(17 3 27)-(3 3 2)	8358.12723(24)	10125.03961(24)	0.4114941(11)	1.53312(82)	-	0.66	41/47	P29/R35	14	2
5331f-0330f		8358.12804(22)	10125.04026(22)	0.41148339(93)	1.5084(73)	-	0.54	38/44	P29/R35	14	2
5221e-0220e	(16 2 27)-(2 2 2)	8365.17455(16)	9542.91922(16)	0.41082219(84)	1.0658(80)	-	0.67	62/66	P36/R22	14	2
5221e-0220f								8/8	Q10	14	2
5221f-0220f		8365.17472(13)	9542.91939(13)	0.41082286(76)	1.1005(73)	-	0.57	61/66	P23/R33	14	2
5221f-0220e								10/11	Q14	14	2
5111e-0110e	(15 1 12)-(1 1 1)	8370.995166(43)	8959.763036(43)	0.40897225(16)	1.8029(14)	1.412(30)	0.31	152/155	P39/R59	14	2
5111e-0110f								31/36	Q24	14	2
5111f-0110f		8370.995047(56)	8959.762917(56)	0.41101654(25)	1.7777(24)	2.892(57)	0.39	153/154	P41/R55	14	2
5111f-0110e								39/40	Q36	14	2
5001e-0000e	(14 0 14)-(0 0 1)	8376.349780(41)	8376.349780(41)	0.40893713(13)	2.15023(98)	5.113(19)	0.28	197/200	P43/R61	14	2
0802e-0110e	(16 0 14)-(1 1 1)	8380.06955(79)	8968.83742(79)	0.4128238(32)	5.492(34)	-	0.62	7/8	R28	15	
0802e-0110f								5/5	Q28	15	
0822e-0110e	(16 2 11)-(1 1 1)	8388.80465(94)	8977.57252(94)	0.4130452(43)	0.465(33)	-	0.99	8/9	R34	15	
0822f-0110f		8388.80618(41)	8977.57405(41)	0.4130242(17)	2.512(12)	-	0.58	14/19	R36	15	
3601e-1000e	(16 0 20)-(2 0 2)	8405.178795(76)	9690.082135(76)	0.40871239(42)	0.2578(51)	11.04(16)	0.45	133/143	P43/R48	14	2
3421e-0000e	(14 2 46)-(0 0 1)	8414.80622(19)	8414.80622(19)	0.41121533(44)	1.3324(26)	6.283(42)	0.59	123/139	P59/R64	14	2
3711e-1110e	(17 1 20)-(3 1 2)	8421.41773(22)	10301.68347(22)	0.4077352(16)	0.778(24)	-	0.57	42/50	P26/R25	14	2
3711f-1110f		8421.41799(27)	10301.68373(27)	0.4102787(14)	0.109(16)	-	0.62	38/60	P26/R30	14	2
0712e-0000e	(15 1 15)-(0 0 1)	8425.02439(17)	8425.02439(17)	0.41147203(60)	2.4479(37)	-	0.71	71/83	P27/R40	15	2
0712f-0000e		8425.02397(15)	8425.02397(15)	0.41365445(43)	2.7074(22)	-	0.58	54/63	Q46	15	2
0(16)00e-0200e	(16 0 32)-(2 0 1)	8430.97069(45)	9599.10299(45)	0.4155221(61)	11.18(22)	-	0.73	35/47	P26/R23	14	2
0(16)20e-0220e	(16 2 27)-(2 2 2)	8432.12642(58)	9609.87109(58)	0.4158124(36)	-6.235(59)	-	0.79	33/42	P34/R36	14	2
0(16)20f-0220f		8432.12567(51)	9609.87034(51)	0.4158266(19)	3.816(14)	-	0.73	/19	P37/R30	14	2

6001e-0200e	(16 0 32)-(2 0 1)	8438.20127(89)	9606.33357(89)	0.407279(11)	2.813(35)	-	0.62	13/14	P25/R25	14							
3401e-0000e	(14 0 15)-(0 0 1)	8452.635884(60)	8452.635884(60)	0.40903577(18)	0.3797(13)	6.245(21)	0.42	192/226	P65/R68	14	2,4						
6310e-0110e	(15 1 15)-(1 1 1)	8452.87658(12)	9041.64445(12)	0.41354259(78)	4.032(11)	17.34(42)	0.49	77/83	P38/R43	14	2						
6310f-0110f		8452.87623(16)	9041.64410(16)	0.4176919(10)	4.343(15)	-7.32(57)	0.64	97/102	P43/R36	14	2						
3511e-0110e	(15 1 16)-(1 1 1)	8472.57403(65)	9061.341901(65)	0.40866329(26)	1.0855(23)	3.208(55)	0.44	/100	P55/R54	14	2						
3511e-0110f								/11	Q13	14	2						
3511f-0110f		8472.57381(71)	9061.341676(71)	0.41068187(31)	0.6135(29)	4.023(71)	0.47	161/179	P58/R56	14	2						
3511f-0110e								24/25	Q15	14	2						
6200e-0000e	(14 0 17)-(0 0 1)	8475.72596(10)	8475.72596(10)	0.41548894(43)	8.3107(43)	62.79(12)	0.50	152/164	P52/R50	14	2						
3621e-0220e	(16 2 35)-(2 2 2)	8484.52589(18)	9662.27056(18)	0.4103115(12)	1.781(21)	-8.24(10)	0.68	76/92	P41/R42	14	2						
3621e-0220f								7/12	Q11	14	2						
3621f-0220f								8484.52534(29)	9662.27001(29)	0.4103144(46)	0.411(16)	-	0.69	34/45	P28/R21	14	2
3621f-0220e														6/8	Q11	14	2
0204e-1000e	(18 0 1)-(2 0 2)	8485.73196(19)	9770.63529(19)	0.4064341(11)	2.601(16)	4.79(55)	0.78	87/98	P43/R44	16	2						
0444e-0440e	(20 4 4)-(4 4 4)	8489.55949(53)	10845.81192(53)	0.408015(13)	1.729(57)	-	0.67	12/12	P42/R37	16	5						
0444f-0440f		8489.56061(81)	10845.81303(81)	0.408014(11)	1.702(61)	-	0.59	13/15	P39/R34	16	5						
3731e-0330e	(17 3 35)-(3 3 2)	8491.4621(11)	10258.3745(11)	0.4108183(50)	1.264(39)	-	0.80	6/8	P33/R33	14							
3731f-0330f		8491.46679(73)	10258.37903(73)	0.4108163(41)	1.295(43)	-	0.65	9/11	P30/R28	14							
0424e-0420e	(20 2 3)-(4 2 3)	8493.76778(74)	10824.88929(74)	0.407577(26)	0.58(33)	-	0.75	12/14	P35/R21	16	5						
0424f-0420f		8493.76989(51)	10824.89134(51)	0.407603(17)	1.878(84)	-	0.59	10/13	P34/R35	16	5						
0404e-0400e	(20 0 2)-(4 0 2)	8497.5299(22)	10820.1030(22)	0.404823(13)	-11.83(19)	-383.8(84)	0.54	10/13	P23/R36	14							
3202e-0110e	(16 0 25)-(1 1 1)	8519.55279(38)	9108.32066(38)	0.4103549(34)	4.905(47)	103.1(17)	0.69	13/17	P11/R40	15							
3202e-0110f								8/11	Q37	15							
3601e-0200e	(16 0 20)-(2 0 1)	8521.94982(17)	9690.08212(17)	0.4087126(12)	0.238(21)	13.11(98)	0.54	82/105	P39/R37	14	2						
3222e-0110e	(16 2 13)-(1 1 1)	8532.47629(41)	9121.24416(41)	0.4107263(21)	0.575(18)	-	0.54	0/1	P17	15							
3222e-0110f								13/13	Q33	15							
3222f-0110f								8532.47384(47)	9121.24171(47)	0.4107364(23)	1,985(21)	-	0.46	12/13	Q31	15	
3222f-0110e														0/2	P19	15	
0115e-0111e	(15 1 2)-(5 1 1)	8535.5869(20)	11333.8795(20)	0.403015(19)	4.25(48)	-	0.72	7/9	P30/R14	16							
0115f-0111f		8538.5838(15)	11333.8764(15)	0.404027(14)	8.41(30)	-	0.85	9/11	P34/R16	16							
0334e-0330e	(19 3 2)-(3 3 2)	8545.04817(12)	10311.96055(12)	0.40731249(33)	1.6440(15)	-	0.65	98/111	P47/R49	16	2						
0334e-0330f								12/16	Q21	16	2						
0334f-0330f								8545.04811(12)	10311.96035(12)	0.40731679(53)	1.7099(55)	3.87(15)	0.57	93/107	P42/R52	16	2
0334f-0330e														14/20	Q21	16	2
1114e-1110e	(19 1 4)-(3 1 2)	8547.66309(57)	10427.92884(57)	0.4037569(22)	1.638(15)	-	0.84	13/19	P38/R1	16	2						
1114f-1110f		8547.66234(45)	10427.92808(45)	0.4045916(13)	1.6821(78)	-	0.68	18/27	P40/R22	16	2						
0(14)20e-0000e	(14 0 46)-(0 0 1)	8487.8307(15)	8487.8307(15)	0.415882(30)	-2.258(17)	-47.76(27)	0.62	13/24	P46/R59	14							
0314e-0310e	(19 1 1)-(3 1 1)	8547.97518(12)	10297.04041(12)	0.40629448(45)	2.1112(28)	-	0.59	92/102	P42/R39	16	2						

0314f-0310f		8547.97476(10)	10297.03991(10)	0.40770316(29)	2.2569(14)	-	0.55	111/123	P49/R45	16	2
3112e-0000e	(15 1 8)-(0 0 1)	8559.18235(18)	8559.18235(18)	0.4092941(14)	2.261(25)	32.6(12)	0.65	84/98	P38/R37	15	2
3112f-0000e		8559.18255(28)	8559.18255(28)	0.4109372(29)	2.186(75)	50.6(54)	0.39	37/39	Q29	15	2
7200e-0200e	(16 0 21)-(2 0 1)	8578.42577(31)	9746.55807(31)	0.4132762(21)	7.8193(33)	51.6(14)	0.60	46/54	P41/R29	14	2
7220e-0220e	(16 2 38)-(2 2 2)	8583.56299(72)	9761.30766(72)	0.4137603(54)	-2.02(12)	-	0.64	10/15	P36/R30	14	
7220f-0220f		8583.55573(60)	9761.30039(60)	0.4137772(19)	2.345(12)	-	0.67	11/16	P40/R15	14	
8000e-1000e	(16 0 22)-(2 0 2)	8589.39307(19)	9874.29641(19)	0.4108201(12)	4.686(21)	17.74(87)	0.56	60/76	P43/R38	14	2
0005e-0001e	(20 0 1)-(4 0 1)	8591.48746(54)	10815.24424(54)	0.4043925(42)	19.059(94)	459.7(54)	0.83	36/49	P36/R20	16	2
7110e-0110e	(15 1 17)-(1 1 1)	8596.92962(12)	9185.69748(12)	0.41160589(53)	3.0592(55)	6.89(15)	0.52	104/122	P54/R44	14	2
7110f-0110f		8596.92908(13)	9185.69695(13)	0.41519148(72)	3.3174(88)	1.06(28)	0.53	93/106	P48/R38	14	2
0224e-0220e	(18 2 2)-(2 2 2)	8600.958600(98)	9778.703270(98)	0.40662032(41)	1.2184(29)	-2.734(57)	0.57	104/158	P62/R54	16	6
0224e-0220f								14/18	Q18	16	
0224f-0220f		8600.958927(87)	9778.703596(87)	0.40661714(22)	1.14758(78)	-	0.61	97/111	P59/R22	16	
0224f-0220e								21/22	Q17	16	
0204e-0200e	(18 0 1)-(2 0 1)	8602.502996(78)	9770.635296(78)	0.40643217(27)	2.5761(21)	4.08(42)	0.40	158/171	P62/R54	16	2
0314e-1110e	(19 1 1)-(3 1 2)	8416.77635(40)	10297.04209(40)	0.4062877(24)	2.032(24)	-	0.53	9/11	P8/R30	16	
0314f-1110f		8416.77496(37)	10297.04070(37)	0.4076995(17)	2.242(13)	-	0.47	12/18	P21/R34	16	
1004e-1000e	(18 0 4)-(2 0 2)	8603.66282(21)	9888.56616(21)	0.40335265(26)	1.8637(25)	3.64(22)	0.99	57/128	P58/R54	16	7
6200e-0000e	(14 0 17)-(0 0 1)	8612.948264(51)	8612.948264(51)	0.41313023(24)	5.0119(21)	20.625(50)	0.31	113/117	P57/R11	14	2
6220e-0000e	(14 2 61)-(0 0 1)	8631.1326(18)	8631.1326(18)	0.4138725(39)	-0.219(26)	-12.79(50)	0.45	12/16	P55	14	
0004e-0000e	(16 0 1)-(0 0 1)	8714.16345(19)	8714.16345(19)	0.40516923(78)	1.74441(76)	-	0.48	31/35	P86	16	2
0623e-0220e	(15 1 17)-(1 1 1)	8634.71236(97)	9802.84466(97)	0.4113955(43)	-0.277(51)	-	0.68	20/24	P44	16	2
0623f-0220f		8634.70920(97)	9802.84149(97)	0.4114151(30)	3.317(20)	-	0.53	13/17	P36	16	2
0603-0200e	(18 0 2)-(2 0 1)	8637.643889(11)	9805.77619(11)	0.4114824(38)	6.293(35)	48.76(93)	0.63	26/37	P48	16	2
0114e-0110e	(17 1 1)-(1 1 1)	8657.317217(25)	9246.08509(25)	0.40553160(21)	1.77914(39)	-	0.39	69/74	P72	16	2
0114f-0110f		8657.31920(39)	9246.08707(39)	0.40627619(35)	1.80288(70)	-	0.53	63/65	P69	16	2
<b><sup>14</sup>N<sup>15</sup>N<sup>16</sup>O isotopologue</b>											
5001e-0000e	(14 0 14)-(0 0 1)	8364.70560(19)	8364.70560(19)	0.40709930(67)	1.2404(58)	5.29(14)	0.66	90/99	P34/R55	14	2
4311e-0110e	(15 1 16)-(1 1 1)	8376.53244(94)	8951.96609(94)	0.4072326(45)	1.116(45)	-	0.39	9/10	P29	14	
4311f-0110f		8376.53256(23)	8951.96620(23)	0.4078566(78)	1.114(61)	-	0.67	9/9	P32	14	
0204e-0200e	(18 0 1)-(2 0 1)	8432.39455(31)	9576.72793(31)	0.4068766(21)	2.911(26)	-	0.62	21/26	P31/R12	16	
0224e-0220e	(18 2 2)-(2 2 2)	8431.00918(39)	9582.04009(39)	0.4069740(14)	0.8679(85)	-	0.65	13/20	P41/R22	16	
0224f-0220f		8431.00927(43)	9582.04017(43)	0.4069759(15)	1.8166(83)	-	0.58	11/12	P42/R30	16	
0114e-0110e	(17 1 1)-(1 1 1)	8484.55849(14)	9059.99214(14)	0.40592390(62)	1.7532(62)	-0.16(12)	0.54	93/129	P51/R49	16	2
0114e-0110f								1/4	Q9	16	
0114f-0110f		8484.55824(13)	9059.99189(13)	0.40668043(29)	17769(13)	-	0.57	94/122	P51/R49	16	2
0114f-0110e								2/3	Q17	16	

0004e-0000e	(16 0 1)-(0 0 1)	8538.510486(52)	8538.510486(52)	0.405623501(92)	1.74231(29)	-	0.41	196/202	P58/R60	16	
<b><sup>15</sup>N<sup>14</sup>N<sup>16</sup>O isotopologue</b>											
3401e-0000e	(14 0 15)-(0 0 1)	8372.786910(98)	8372.786910(98)	0.39620985(63)	0.1757(95)	2.41(37)	0.47	104/117	P43/R42	14	2
0114e-0110e	(17 1 1)-(1 1 1)	8571.99260(12)	9157.30472(12)	0.39176682(25)	1.67320(96)	-	0.50	77/85	P46/R56	16	2
0114f-0110f		8571.99275(14)	9157.30487(14)	0.39246993(28)	1.7089(11)	-	0.55	66/90	P57/R47	16	2
0224e-0220e	(18 2 2)-(2 2 2)	8515.77714(25)	9686.62014(25)	0.3928104(17)	1.773(17)	-	0.55	15/17	P33/R23	16	
0224f-0220f		8515.77610(74)	9686.61910(74)	0.3928078(31)	1.248(22)	-	0.88	9/9	P14/R36	16	
0204e-0200e	(18 0 1)-(2 0 1)	8517.34616(25)	9677.31787(25)	0.39258957(91)	2.2431(61)	-	0.76	33/44	P42/R38	16	
0004e-0000e	(16 0 1)-(0 0 1)	8628.68348(12)	8628.68348(12)	0.39141029(29)	1.6738(18)	0.58(29)	0.39	90/99	P67	16	2
3511e-0110e	(15 1 16)-(1 1 1)	8395.10391(36)	8980.41603(36)	0.3956188(13)	0.8629(78)	-	0.60	16/18	P32/R38	14	
3511f-0110f		8395.10427(52)	8980.41639(52)	0.3976831(21)	0.484(14)	-	0.86	16/18	P26/R37	14	
<b><sup>14</sup>N<sub>2</sub><sup>18</sup>O isotopologue</b>											
6200e-0000e	(14 0 17)-(0 0 1)	8428.79738(16)	8428.79738(16)	0.38939701(72)	3.1348(58)	-	0.59	56/64	P35/R35	14	
7000e-0000e	(14 0 18)-(0 0 1)	8520.97341(18)	8520.97341(18)	0.38762547(77)	1.1502(64)	-	0.71	76/98	P36/R35	14	
0004e-0000e	(16 0 1)-(0 0 1)	8681.69797(72)	-	-	-	-		/8	P62	16	8
<b><sup>15</sup>N<sub>2</sub><sup>16</sup>O isotopologue</b>											
0004e-0000e	(16 0 1)-(0 0 1)	8450.30474(43)	8450.30474(43)	0.3918582(13)	1.6319(76)	-	0.73	17/22	P36/R41	16	

## Notes

The confidence interval (1SD) is in the units of the last quoted digit.

<sup>a</sup>  $V_1 V_2 I_2 V_3$  correspond to the maximum value of the modulo of the expansion coefficients of the eigenfunction.  $V_2$  is given between parenthesis when it is larger than 10.

<sup>b</sup> Cluster labelling notation: ( $P=2V_1+V_2+4V_3, I_2, i$ ),  $i$  is the order number within the cluster increasing with the energy.

<sup>c</sup>  $\Delta G_v = G_v' - G_v''$  is the band center.

<sup>d</sup> Root Mean Square of the (Obs.-Calc.) differences of the position values ( $10^{-3} \text{ cm}^{-1}$ ).

<sup>e</sup>  $N_{fit}$  is the total number of transitions included in the fit;  $N_{obs}$  is the total number of measured transitions of the considered band.

<sup>f</sup> Observed branch with the maximum value of the total angular momentum quantum number of the input data.

<sup>g</sup>  $\Delta P = P' - P''$ , where  $P'$  and  $P''$  are the upper and lower polyads.

<sup>h</sup> Notes: 1 – Measured line positions from Ref.[1] were included in the fit; 2 – Measured line positions from Ref. [17] were included in the fit; 3 - Anharmonic intrapolyad interaction (16 0 9)  $\leftrightarrow$  (16 0 18) at  $J=29$ ; 4 – Coriolis Interpolyad interaction (14 0 15)  $\leftrightarrow$  (15 3 23) at  $J=51$ ; 5 – Low constants 0420e/0420f and 0440e/0440f were fitted (See Supplementary Material II); 6 - Intrapolyad anharmonic interaction (18 2 2)  $\leftrightarrow$  (16 2 38) at  $J=47$ ; 7 - Intrapolyad anharmonic interaction (18 0 4)  $\leftrightarrow$  (18 0 3) at  $J=14$ , Coriolis Interpolyad interaction (18 0 4)  $\leftrightarrow$  (17 1 10)  $J=34$ , Intrapolyad anharmonic interaction (18 0 4)  $\leftrightarrow$  (16 0 2) at  $J=45$ ; 8 – The band center of the 0004e-0000e band (448 isotopologue) provided by the global effective Hamiltonian;